An Automatic Neutral Section Power Supplier Serving as Railway Power Conditioner on Time-Division Basis

Zhibo Zhang, *Graduate Student Member, IEEE*, Trillion Q. Zheng, *Senior Member, IEEE*, Changyu Gao, *Graduate Student Member, IEEE*, Kai Li, *Member, IEEE*, and Jiawei Guo

***Abstract*—To address the issue of brief power outages when trains pass through the neutral section, various automatic neutral section power suppliers have been investigated. However, the schemes in existing literature have two main problems: the converter has numerous bridge legs and large capacity, and only operates briefly during trains passing through the neutral section, remaining in standby and idle state for over 95% of the time. To solve these two problems, this article proposes a converter topology for an automatic neutral section power supplier based on a three-leg converter. The proposed topology has fewer bridge-leg counts and requires a smaller converter capacity. By simply adding an ac switch and an inductor, it functions as a railway power conditioner, utilizing the automatic neutral section power supplier's idle time on time-division basis to improve the traction power supply quality. This article provides a detailed analysis of the coupling relationship and decoupling control methods of the input and output of the proposed topology when used as an automatic neutral section power supplier, as well as the control logic when used as a railway power conditioner. The effectiveness of the proposed system has been verified by simulation results and the experimental results of a down-scaled prototype.**

***Index Terms*—Automatic neutral section power supplier (ANSPS), electric railway, neutral section, power decouple, power quality.**

NOMENCLATURE

$u_{\rm A}$, $u_{\rm B}$, $u_{\rm C}$	Phase A, B, and C voltages of the power grid.
u_α, u_β	Voltages of the traction feeders α and β.
$u_{\rm ao}$, $u_{\rm bo}$, $u_{\rm co}$	Output voltages of phase a, b and c leg.
$u_{\rm dc}$	Voltage of dc bus.
$u_{\rm ag}$, $u_{\rm bg}$, $u_{\rm cg}$, $u_{\rm og}$	Potentials at points a, b, c, and o.
$u_{\rm N}$	Voltage of neutral section catenary.
$i_{\rm a}$, $i_{\rm b}$, $i_{\rm c}$	Currents of phase a, b, and c leg.
$i_{\rm A}$, $i_{\rm B}$, $i_{\rm C}$	Phase A, B, and C currents of the power grid.
$i_{\rm A}'$, $i_{\rm B}'$, $i_{\rm C}'$	Grid currents after compensation.
i_α, i_β	Traction transformer currents of feeders α and β.
$i_{\alpha{\rm c}}$, $i_{\beta{\rm c}}$, $i_{\rm cc}$	Compensation currents of a, b, and c leg.
$i_{\alpha{\rm L}}$, $i_{\beta{\rm L}}$	Traction currents of feeder α and β.
$T_{\rm trans}$	Current transfer time when pantograph overlapping catenaries.
$T_{\rm shift}$	Phase shift time of neutral section voltage.
$L_{\rm a}$, $L_{\rm b}$, $L_{\rm c}$	Inductors of phase *a*, *b*, and *c* leg.
$\theta_{\rm AB}$	Phase angle difference of the voltage of feeder α and β.
$\theta_{\rm AC}$	Phase shift angle of neutral section voltage.

Manuscript received 5 December 2023; revised 19 March 2024; accepted 20 April 2024. Date of publication 29 April 2024; date of current version 20 June 2024. This work was supported by the National Natural Science Foundation of China under Grant 52007005. Recommended for publication by Associate Editor D. Dujic. *(Corresponding author: Kai Li.)*

The authors are with the School of Electrical Engineering, Beijing Jiaotong University, Beijing 100044, China (e-mail: zbzhang@bjtu.edu.cn; tqzheng@bjtu.edu.cn; 21117028@bjtu.edu.cn; kaili@bjtu.edu.cn; 16291026@bjtu.edu.cn).

Color versions of one or more figures in this article are available at https://doi.org/10.1109/TPEL.2024.3394741.

Digital Object Identifier 10.1109/TPEL.2024.3394741

I. INTRODUCTION

THE 25 kV 50 Hz single-phase traction power supply system of electrified railway is used worldwide. The three-phase public grid voltage is stepped down by the traction transformer to power the traction network [1]. Since the electric locomotive is a single-phase load, in order to reduce the unbalance of the three-phase grid load, the catenary is segmented and various traction feeders are powered by alternate phase voltages cyclically [2]. A neutral section, which is also named the electrical phase separation section, is correspondingly set between two traction feeders to avoid interphase short circuit [3].

At present, the train passing through a phase separation section without power supply is a main way for ac electrified railway. The train would slide across the neutral section by the action of inertia. The train could have to stop in the neutral section as the speed drops to zero, especially on uphill railways. In addition, due to the influence of distributed inductance and capacitance [4], the transient overvoltage may occur when the pantograph is overlapping the traction feeder and neutral section, and an arc will be generated between the pantograph and the catenary [5]. This interrupted power phase-separation passing scheme limits the further development of electrified railway. In order to solve these issues, a switch-type automatic phase-passing system is proposed [6]. The power interruption time of the train is greatly shortened. Even so, the dc undervoltage protection of the locomotive may occur during the power outage time [7]. In order to completely eliminate the power outage time, the cophase traction power supply scheme is proposed to replace the traditional traction power supply system. The voltage phase of the whole railway line is consistent, and the electric phase

separation can be canceled [8], [9]. The cophase traction power supply system based on three-phase to single-phase converter is common [10], [11], and there is also cophase power supply system based on modular multilevel converter (MMC), some of which are applied in an autotransformer-fed power supply system [12]. However, the converter capacity of the cophase power supply system needs to meet the total power of all locomotives in the whole railway line, which results in high cost.

An automatic neutral section power supplier (ANSPS) can provide uninterruptible power supply for the neutral section at a rather lower cost [13]. This scheme can realize the smooth transition of the neutral section voltage between the traction feeders. The ANSPSs are mostly based on back-to-back single-phase converters at first [14], [15], and then the phase-shifting transformer composed of two transformers in series is introduced into the system and retained in subsequent research [16]. It can reduce the converter capacity of the inverter side. However, compared to passing through the whole feeding section of a traction power substation, the train takes very short time to pass the neutral section, and the converter has to be in the standby state for more than 95% of the time, so the equipment utilization rate is too low. In addition, there are problems of reactive power and negative sequence current on the grid side [17]. A railway power conditioner (RPC) is usually employed to compensate reactive power and negative sequence current in the grid [18]. RPC can use a variety of topologies, such as MMC or cascaded H-bridge topology to achieve transformerless [19], [20]. RPC can only carry out power quality improvement and cannot provide uninterrupted power supply for trains running in the neutral section. In order to have both functions, a common way is to add a part of additional converter to the original ANSPS to realize the power quality improvement [22]. A scheme based on back-to-back single-phase converter with an additional converter port is presented in [23]. An ANSPS based on MMC with power quality improvement function is proposed [21], [27]. But the converter capacity in these two schemes is rather large. There are also schemes that use a three-phase converter at the rectifier side and two transformers connected in series to reduce the converter capacity [24]. Compared with other schemes, the scheme in [24] is a pretty good scheme with smaller converter capacity and complete functions. However, the train takes very short time to pass the neutral section, compared to passing through the whole feeding section of a traction power substation, and the inverter side converter has to be in the standby state for more than 95% of the time [25].

Many schemes of trains passing through a phase separation section have been proposed, their advantages and disadvantages are shown in Fig. 1. In the existing scheme, the converter capacity is still very large, and the converter in the system is idle for a large part of the time. In order to solve these problems, this article proposes a converter topology for ANSPS based on a three-leg converter. The newly proposed converter topology has a reduced number of bridge legs and a lower output voltage on each leg. Consequently, this results in a smaller converter capacity requirement when employed as an ANSPS. This topology simply adds an ac switch and an inductor connected in series to one ac terminal of a conventional three-phase converter,

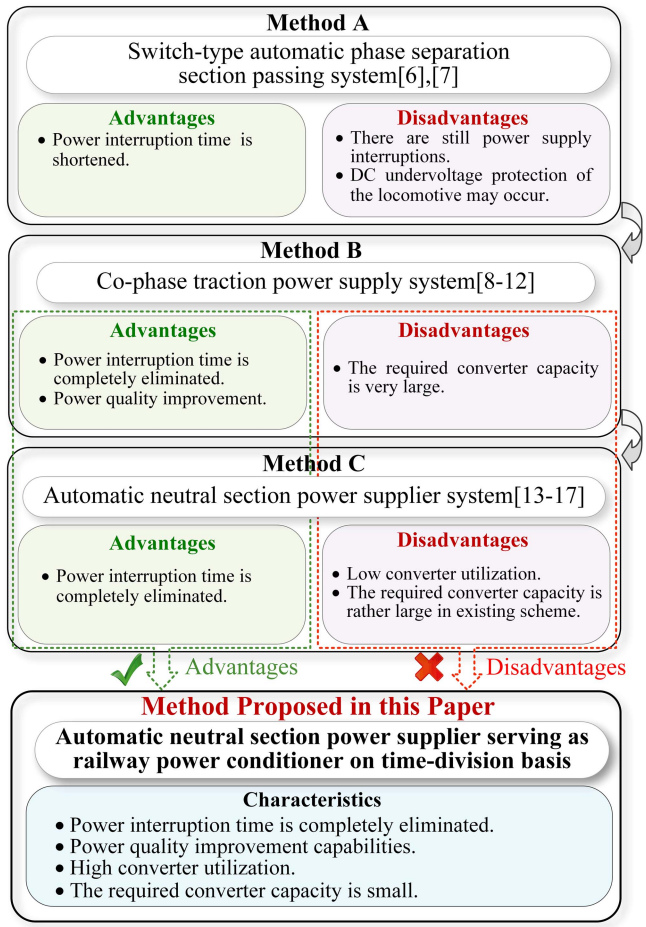

Fig. 1. Advantages and disadvantages of various schemes of trains passing through a phase separation section.

enabling it to function as an RPC. It utilizes the idle time of the ANSPS on time-division basis to improve the power quality of a traction power supply. The utilization rate of the converter can be significantly enhanced.

The rest of this article is organized as follows. In Section II, the configuration of the ANSPS system is presented and the circuit is analyzed in detail. In Section III, the operation principle of the system is analyzed and the control strategy for the whole process of the system is proposed. In Section IV, the scheme proposed in this article is compared with other schemes in terms of converter capacity. In Sections V and VI, the effectiveness and the superiority of ANSPS are verified by both the simulation and the experimental results of a laboratory low-power prototype. Finally, Section VII concludes this article.

II. System Configuration and Circuit Analysis

A. System Configuration

The configuration of an ANSPS system proposed in this article is shown in Fig. 2. The three-phase voltage of the power grid is transformed into two single-phase voltages by the traction transformer in the traction substation. The traction transformer

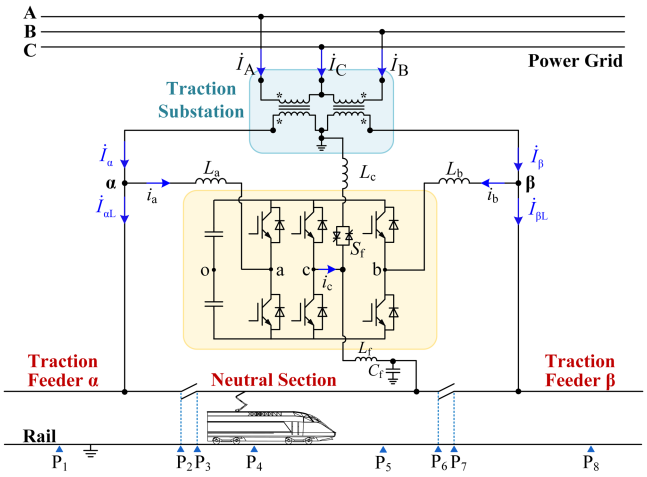

Fig. 2. Proposed ANSPS system.

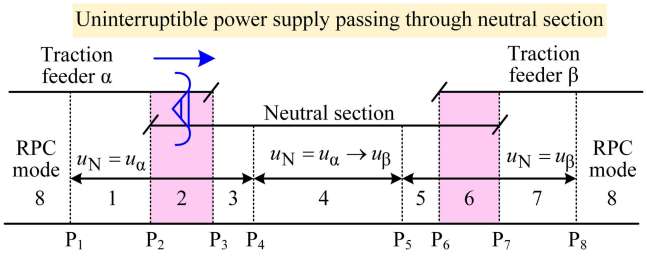

Fig. 3. Schematic diagram of whole process of system.

can adopt V/v transformer, Scott transformer, or other transformers [26]. In this article, the V/v transformer is used in traction substation, so the phase angle difference between the voltage of the traction feeders α and β is $\pi/3$. The system is mainly composed of a three-leg power electronic converter. The three legs of the converter are phase a leg, phase b leg, and phase c leg, respectively, and the virtual midpoint of the dc bus is o. The phase a leg and phase b leg are connected to the traction feeders α and β through two inductors L_a and L_b. The phase c leg is connected to the neutral section catenary through a filter, which consists of L_f and C_f. The dc midpoint is insulated from the ground, and the two legs of the converter jointly bear the voltage between the catenaries and the ground. Due to the high voltage of the catenary, in practical engineering, the converter should adopt a multilevel topology, and the MMC or other suitable multilevel topology can be adopted. If the output voltage harmonics of the multilevel converter meet the actual demand, the filter of phase c leg can be omitted. In this article, in order to facilitate the description, the two-level structure is used to simplify the representation circuit without affecting the circuit principle. For the purpose of improving the converter utilization rate, when there are no trains passing through the neutral section, the converter serves as an RPC. In order to improve the power quality of the power grid, the system needs to add a path to the ground, so the phase c leg of the converter is connected to the ground through an ac switch S_f and an inductor L_c. The ac switch S_f, called function selector, can adopt a series of thyristor valve group or high-voltage circuit breaker. The inductance L_c is the same as the inductance of L_a and L_b. The circuit structure is altered by the action of the function selector switch S_f to achieve time-division multiplexing of the converter.

There are many methods to detect the position of the train. As one of the feasible methods, laser radar is selected as the sensor to detect the train location. The sensors are installed at points P_1–P_8. According to the train location information, the whole process control of the system is carried out. When the train passes the neutral section, S_f is at OFF state, and the neutral section catenary is powered by the ANSPS system. When the train runs on the railway outside of the neutral section, S_f is at ON state and the power quality improvement of the traction substation is administered.

B. Whole Process of the Proposed System

In this system, the whole process is divided into two working modes: ANSPS mode and RPC mode. Depending on the location of the train, the two modes are further divided into eight stages, corresponding to the following eight serial numbers, as shown in Fig. 3. Taking the train traveling from the left to the right as an example, before the train reaches point P_1, the system is in the RPC mode.

1) After the train reaches point P_1, the function selector switch S_f is turned OFF, and the system enters the ANSPS mode. When the train is traveling between P_1 and P_2, the output voltage is controlled to track the voltage of the traction feeder α, thereby reducing even eliminating the arc between the pantograph and the catenary when the pantograph travels to point P_2.
2) When the train reaches point P_2, the output power of the converter begins to increase gradually. When the pantograph and the traction feeder α are separated at point P_3, there is no current transmitted from the traction feeder α to the pantograph, avoiding the instantaneous overvoltage problem.
3) When the train reaches point P_3, all traction power comes from the converter. The voltage of the neutral section catenary is consistent with the voltage of the traction feeder α, when the train is located between P_3 and P_4.
4) When the train reaches point P_4, the phase of output voltage begins to change gradually. The voltage of the neutral section catenary is smoothly switched to the traction feeder β. Before the train arrives at point P_5, the voltage of the neutral section catenary has been adjusted to match the voltage of the traction feeder β.
5) When the train is traveling between P_5 and P_6, the output voltage is controlled to track the voltage of the traction feeder β to reduce or eliminate the arc between the pantograph and the catenary, when the pantograph travels to point P_6.
6) When the train reaches point P_6, the output power of the converter begins to reduce gradually. The output power is reduced to zero before the train reaches point P_7.
7) When the train reaches point P_7, all traction power of the train comes from the traction feeder β. The phase c leg of the converter is blocked.

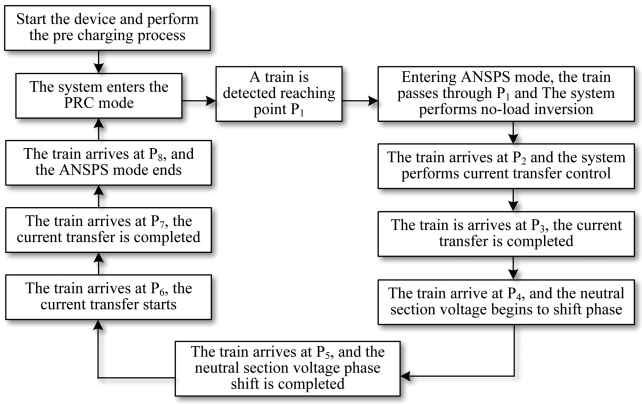

Fig. 4. Status flowchart of whole process of system.

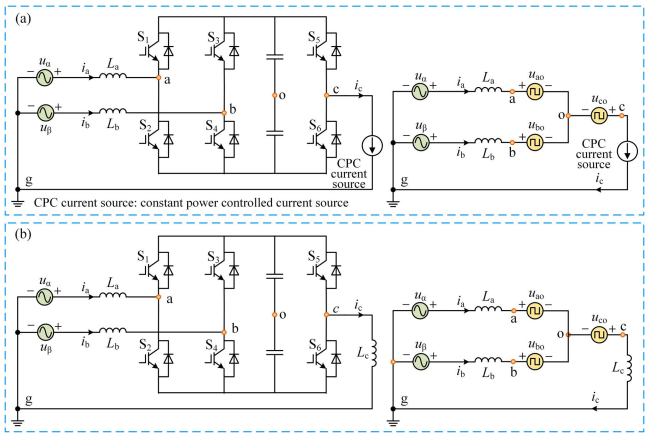

Fig. 5. Circuit diagram and equivalent model of the proposed system. (a) Circuit diagram and equivalent model in ANSPS mode. (b) Circuit diagram and equivalent model in RPC mode.

8) When the train reaches point P_8, the function selector switch S_f is turned ON, and the system enters the RPC mode.

This is the whole process of the ANSPS system, the status flow chart is shown in Fig. 4, the train can get uninterrupted power supply throughout the whole journey. In order to achieve such control, the circuit needs to be further analyzed.

C. Circuit Analysis and Modeling

The circuit structure of the system in two working modes is different, so the equivalent circuit of the system is divided into two types, as shown in Fig. 5, where the impedance of the wires between the traction transformer and the converter is neglected. u_α and u_β represent the voltages of the traction feeders α and β. $u_{\rm ag}$, $u_{\rm bg}$, $u_{\rm cg}$, and $u_{\rm og}$ are the potentials at points a, b, c, and o, with ground g considered as the potential reference zero. $i_{\rm a}$, $i_{\rm b}$, and $i_{\rm c}$ represent the phase currents of the converter. $u_{\rm ao}$, $u_{\rm bo}$, and $u_{\rm co}$ are the output voltages of phase a leg, phase b leg, and phase c leg. Each leg of the converter can be equivalent to a controlled voltage source. The external port characteristics of the locomotive resemble that of a constant power controlled (CPC) current source. The circuit structures in Fig. 5(a) and (b) are similar, but their control objectives are fundamentally different. In the state of Fig. 5(a), the control objective of the converter is to output a suitable voltage $u_{\rm cg}$ for the locomotive. In the state of Fig. 5(b), the control objective of the converter is to transfer a part of the active current between traction feeder α and traction feeder β, and to compensate the appropriate reactive current to ensure the three-phase load balance on the grid side.

In these two equivalent circuits, due to the dc midpoint is insulated from the earth, it is required that the sum of the input-side current in one cycle should be equal to the output-side current. There is

$$\dot{I}_{\rm a} + \dot{I}_{\rm b} = \dot{I}_{\rm c} \tag{1}$$

where $\dot{I}_{\rm a}$, $\dot{I}_{\rm b}$, and $\dot{I}_{\rm c}$ represent the phase currents of the converter, regarding the voltage of traction feeder α to be the phase angle reference zero. It is shown from (1) that there is a coupling relationship between the input current and the output current. These three currents must satisfy such a relationship, in which there are only two independent variables.

In the case of Fig. 5(a), the control objective of the converter is to ensure that $u_{\rm cg}$ meets the power supply demand of the locomotives. $\dot{I}_{\rm c}$ is determined by the traction power of the locomotive, the converter can only provide voltage but cannot control the traction current $\dot{I}_{\rm c}$, which is one of the independent variables of the current. For the input currents $\dot{I}_{\rm a}$ and $\dot{I}_{\rm b}$, due to the current coupling relationship, a change in one of the currents results in a change in the other. The adjustment of the input current will cause a change in the input power. In order to maintain the dc voltage, it is also necessary to control the balance between the input power and the output power. Therefore, the setting of the input current reference value needs to consider both the current coupling relationship and the power balance. Considering that the dc midpoint is not grounded, the potential of the virtual dc midpoint is no longer a fixed value. According to KVL, the potential $u_{\rm og}$ of the dc virtual midpoint should have the following relationship:

$$u_\alpha - L_{\rm a}\frac{{\rm d}i_{\rm a}}{{\rm d}t} - u_{\rm ao} = u_{\rm og} \tag{2}$$

$$u_\beta - L_{\rm b}\frac{{\rm d}i_{\rm b}}{{\rm d}t} - u_{\rm bo} = u_{\rm og}. \tag{3}$$

Through the analysis of (2) and (3), $u_{\rm og}$ is affected by $i_{\rm a}$, $i_{\rm b}$, $u_{\rm ao}$, and $u_{\rm bo}$. Next, analyzing from the output side, $u_{\rm cg}$ can be considered as consisting of two voltage components $u_{\rm co}$ and $u_{\rm og}$. $u_{\rm og}$ should meet this relationship

$$u_{\rm cg} - u_{\rm co} = u_{\rm og} \tag{4}$$

where the $u_{\rm cg}$ is determined by the train's requirements for the traction power system, and $u_{\rm co}$ can be altered directly by controlling the phase c leg of the converter. From (2) to (4), given that the voltages of u_α, u_β, and $u_{\rm cg}$ are predetermined, $u_{\rm og}$ will collectively affect the output voltages of the three legs.

The output voltage is the superposition of the phase c voltage of the converter and the virtual dc midpoint potential. From the input side, the traction feeder voltage minus the output voltage of the corresponding converter leg is the virtual dc midpoint potential. A coupling relationship exists between the

output voltage and the input voltage. Both the input side and the output side are associated with this potential, serving as a link to establish a connection between the input and output voltages. The virtual dc midpoint potential significantly influences the converter; it should not be arbitrary but should possess a reference value. This reference value is achieved by making the virtual midpoint potential follow it through the collaboration of multiple converter legs. The reference value of the virtual midpoint potential is related to the output voltage of each leg. A reasonable reference value of the virtual midpoint potential can reduce the output voltage of each leg.

In the case of Fig. 5(b), the control objective is to adjust the currents $\dot{I}_{\mathrm{a}}$ and $\dot{I}_{\mathrm{b}}$ based on the load condition of the locomotive on the line to balance the three-phase load of the power grid. Achieving this objective involves controlling $\dot{I}_{\mathrm{a}}$ and $\dot{I}_{\mathrm{b}}$, while $\dot{I}_{\mathrm{c}}$ only needs to satisfy the coupling relationship. Therefore, the control process resembles that of the conventional RPC converter. Throughout this process, the virtual midpoint potential also influences the output voltage of the converter leg.

In the conventional ac–dc–ac converter, the input voltage and output voltage are not directly related. The converter can be controlled separately on the rectifier side and the inverter side, the input side, and the output side are decoupled at the intermediate dc link. In the topology shown in Fig. 5(a), the output voltage is partly from the converter and partly from the input voltage. At the same time, the input current and the output current also need to meet (1). Therefore, the converter cannot be controlled independently on the rectifier side and the inverter side, respectively. Instead, it is necessary to propose a three-leg cooperative control method for such a coupling relationship, and the key points of the control are mainly in the following three points.

1) In order to reduce the output voltage of each leg, it is necessary to reasonably select the reference value for the virtual dc midpoint potential. The reference value of the virtual midpoint potential should be selected by considering both working modes comprehensively.
2) In order to maintain the dc voltage of the converter and output the appropriate voltage, it is challenging to analyze the mechanism of cooperative operation of multiple legs in the case of current and voltage coupling.
3) During the train passing through the neutral section, the voltage phase of the catenary is smoothly switched. It is challenging to analyze the influence mechanism of the voltage phase change on the current reference values of the converter input side legs.

In the ANSPS mode, the three key points are all included. In the RPC mode, the control is similar to that of the conventional RPC converter, there is only the problem of dc midpoint potential selection. In the following, these key points will be analyzed in principle.

D. Reference Value of Virtual Midpoint Potential

To facilitate the analysis of the reference value of u_{og}, the voltage drops on the inductors are ignored and a phasor diagram

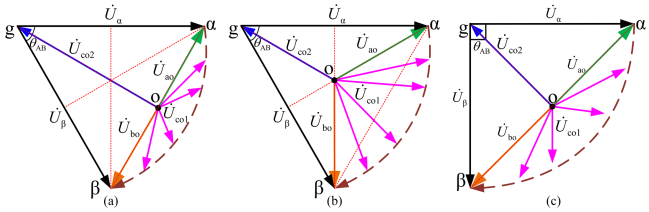

Fig. 6. Phasor diagram of the proposed system. (a) Midpoint potential is at the middle point of the voltage difference between traction feeders when θ_{AB} is 60°. (b) Midpoint potential is at the circumcenter of traction feeder voltages when θ_{AB} is 60°. (c) Midpoint potential is at the circumcenter of traction feeder voltages when θ_{AB} is 90°.

is created with the voltage of traction feeder α as the phase angle reference zero. The phasor diagram is shown in Fig. 6.

The voltage phasors of phase a leg and phase b leg are $\dot{U}_{\mathrm{ao}}$ and $\dot{U}_{\mathrm{bo}}$. The voltage phasor of phase c leg is $\dot{U}_{\mathrm{co1}}$ when in the ANSPS mode and $\dot{U}_{\mathrm{co2}}$ when in the RPC mode. As the train passes through the neutral section, the voltage amplitude of the neutral section catenary does not change and the phase angle moves slowly from one side of the traction feeder to the other side of the traction feeder. Taking the train from traction feeder α to β as an example, in the phasor diagram, the neutral section catenary voltage is represented as a circular arc with the point g as the center of the circle, and the voltage amplitude remains the same as that of the voltage of the two traction feeders. The endpoints of the three-leg voltages $\dot{U}_{\mathrm{ao}}$, $\dot{U}_{\mathrm{bo}}$, and $\dot{U}_{\mathrm{co1}}$ are located at α, β, and the circular arc, respectively. When the system is in the RPC mode, the endpoints of the three-leg voltages $\dot{U}_{\mathrm{ao}}$, $\dot{U}_{\mathrm{bo}}$, and $\dot{U}_{\mathrm{co2}}$ are located at α, β, and g, respectively. The potential of the starting point o of the three-leg voltage phasors, that is, the potential of the virtual midpoint, can determine the amplitude of these voltages. There is a certain freedom in the selection of the reference value of the virtual midpoint potential, and the position of point o can be moved within a certain range. The minimum value of the dc voltage is determined by the maximum leg voltage $U_{\mathrm{leg(max)}}$.

$$U_{\mathrm{leg(max)}} = \max\left\{U_{\mathrm{ao}}, U_{\mathrm{bo}}, U_{\mathrm{co1}}, U_{\mathrm{co2}}\right\}. \tag{5}$$

When the point o is located at the midpoint of the phasor difference between $\dot{U}_{\alpha}$ and $\dot{U}_{\beta}$, and θ_{AB} is 60°, as shown in Fig. 6(a). At this time, the maximum leg voltage is

$$U_{\mathrm{leg(max)}} = U_{\mathrm{co2}} = \frac{\sqrt{3}}{2}U_{\alpha}. \tag{6}$$

When the point o is located at the circumcenter of traction feeder voltages $\dot{U}_{\alpha}$ and $\dot{U}_{\beta}$, as shown in Fig. 6(b) and θ_{AB} is 60°. At this time, the maximum leg voltage is

$$U_{\mathrm{leg(max)}} = U_{\mathrm{ao}} = U_{\mathrm{bo}} = U_{\mathrm{co1}} = U_{\mathrm{co2}} = \frac{\sqrt{3}}{3}U_{\alpha}. \tag{7}$$

When the point o is located at the circumcenter of traction feeder voltages $\dot{U}_{\alpha}$ and $\dot{U}_{\beta}$, as shown in Fig. 6(c) and θ_{AB} is 90°. At this time, the circumcenter of traction feeder voltages $\dot{U}_{\alpha}$ and $\dot{U}_{\beta}$ is the same as the midpoint of the phasor difference

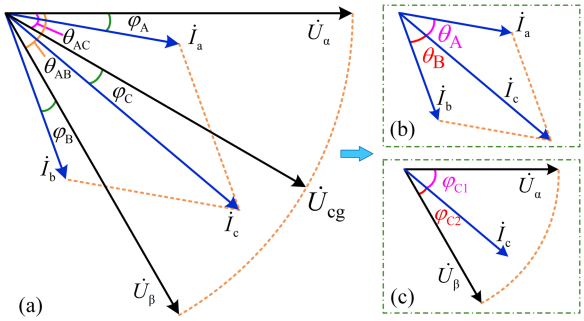

Fig. 7. Phasor diagram of input and output currents and voltages. (a) Phase angle relationships between voltages and currents. (b) Intermediate variable of the phase angles between currents. (c) Intermediate variable relating to the phase angles between the current and the voltages.

between $\dot{U}_\alpha$ and $\dot{U}_\beta$. The maximum leg voltage is

$$U_{\mathrm{leg(max)}} = U_{\mathrm{ao}} = U_{\mathrm{bo}} = U_{\mathrm{co1}} = U_{\mathrm{co2}} = \frac{\sqrt{2}}{2} U_\alpha. \quad (8)$$

The minimum dc voltage required by the converter is determined by the maximum output voltage of each converter leg. Therefore, the objective in selecting the virtual midpoint potential is to minimize the maximum output voltage from the converter's legs. The reference value for the virtual midpoint potential should be chosen at the circumcenter of the triangle formed by the traction feeder voltages. This positioning ensures a balanced voltage output across the three legs, effectively reducing both the maximum leg voltage and the required dc voltage.

III. Operation Principle and Control Strategy

A. ANSPS Mode

In the control of this working mode, the decoupling operation should be carried out according to the existing coupling relationship and power balance relationship, and the reference value for the input current should be solved. However, a deviation in dc voltage occurs due to measurement error or power imbalance in the transient process of the system. To address this, the system should have the dc voltage control ability. Consequently, an analysis of the principles of dc voltage control is conducted. Finally, the system control is conducted based on these derived results.

1) Decoupling Principle: In this part, a decoupling analysis is conducted, expressing the reference value of the input current in terms of known quantities. The phasor diagram in Fig. 7 illustrates the relationships among input and output currents and voltages.

A fundamental condition for the stable operation of the converter is maintaining a constant dc voltage. To ensure this, the input and the output active power of the system should be kept in balance. The system provides the voltage required by the locomotive, the amplitude and the phase of the load current $\dot{I}_\mathrm{c}$ are determined by the traction conditions of the locomotive. The load current $\dot{I}_\mathrm{c}$ is measured by the current transformer at point c in Fig. 2. The balance relationship of the active power can be expressed as follows:

$$U_\alpha I_\mathrm{a} \cos\varphi_\mathrm{A} + U_\beta I_\mathrm{b} \cos\varphi_\mathrm{B} = U_\mathrm{cg} I_\mathrm{c} \cos\varphi_\mathrm{C}. \quad (9)$$

In order to facilitate the calculation, several intermediate angle variables are introduced. The angle between $\dot{I}_\mathrm{a}$ and $\dot{I}_\mathrm{c}$ is expressed as θ_A. The angle between $\dot{I}_\mathrm{b}$ and $\dot{I}_\mathrm{c}$ is denoted as θ_B. The angle between $\dot{I}_\mathrm{c}$ and $\dot{U}_\alpha$ is denoted as φ_{C1}. The angle between $\dot{I}_\mathrm{c}$ and $\dot{U}_\beta$ is denoted as φ_{C2}. The angle between the output voltage $\dot{U}_\mathrm{cg}$ and the traction feeder voltage $\dot{U}_\alpha$ of phase α is called the phase shift angle, which is represented by θ_AC, this angle will change accordingly with the position of the train.

$$\theta_\mathrm{A} = \theta_\mathrm{AC} + \varphi_\mathrm{C} - \varphi_\mathrm{A} \quad (10)$$

$$\theta_\mathrm{B} = \theta_\mathrm{AB} - \theta_\mathrm{AC} - \varphi_\mathrm{C} + \varphi_\mathrm{B} \quad (11)$$

$$\varphi_{\mathrm{C1}} = \theta_\mathrm{AC} + \varphi_\mathrm{C} \quad (12)$$

$$\varphi_{\mathrm{C2}} = \varphi_{\mathrm{C1}} - \theta_\mathrm{AB}. \quad (13)$$

According to the coupling relationship between input and output currents, the input currents can be decomposed into two components: one along the direction of the output current phasor and the other perpendicular to the output current phasor. The sum of the input current components along the output current phasor direction and the output current are equal, and the sum of the input current components in the direction perpendicular to the output current phasor is zero. These relationships can be expressed by the following equations:

$$I_\mathrm{a} \cos\theta_\mathrm{A} + I_\mathrm{b} \cos\theta_\mathrm{B} = I_\mathrm{c} \quad (14)$$

$$I_\mathrm{a} \sin\theta_\mathrm{A} - I_\mathrm{b} \sin\theta_\mathrm{B} = 0. \quad (15)$$

Based on (14) and (15), I_a and I_b can be expressed as follows:

$$I_\mathrm{a} = \frac{\sin\theta_\mathrm{B}}{\sin(\theta_\mathrm{A} + \theta_\mathrm{B})} I_\mathrm{c} \quad (16)$$

$$I_\mathrm{b} = \frac{\sin\theta_\mathrm{A}}{\sin(\theta_\mathrm{A} + \theta_\mathrm{B})} I_\mathrm{c}. \quad (17)$$

Next, (9) can be transformed into

$$I_\mathrm{a} \sin(\theta_\mathrm{A} - \varphi_\mathrm{k}) = \frac{U_\mathrm{cg}\cos\varphi_\mathrm{C} - U_\beta \cos\varphi_{\mathrm{C2}}}{\sqrt{k_1^2 + k_2^2}} I_\mathrm{c} \quad (18)$$

where three intermediate variables are introduced

$$k_1 = U_\alpha \sin\varphi_{\mathrm{C1}} - U_\beta \sin\varphi_{\mathrm{C2}} \quad (19)$$

$$k_2 = -U_\alpha \cos\varphi_{\mathrm{C1}} + U_\beta \cos\varphi_{\mathrm{C2}} \quad (20)$$

$$\varphi_\mathrm{k} = \arctan\left(\frac{k_2}{k_1}\right). \quad (21)$$

Since there are two unknown variables I_a and θ_A in (18), the equation has multiple solutions. A simple and feasible calculation method in engineering is provided here. This calculation method is to make the value of the trigonometric function maximum, so as to obtain the minimum current I_a.

$$|\sin(\theta_\mathrm{A} - \varphi_\mathrm{k})| = 1. \quad (22)$$

Considering that I_a represents the RMS value of the phase a current, it follows $I_\mathrm{a} > 0$. The minimum value of I_a is obtained

as follows:

$$I_{\mathrm{a}}=\frac{\left|\cos\varphi_{\mathrm{C}}-\frac{U_{\beta}}{U_{\mathrm{cg}}}\cos\varphi_{\mathrm{C2}}\right|}{\sqrt{k_1^2+k_2^2}}I_{\mathrm{c}} \tag{23}$$

$$\theta_{\mathrm{A}}=\begin{cases}\varphi_{\mathrm{k}}+\frac{\pi}{2} & \text{when } U_{\mathrm{cg}}\cos\varphi_{\mathrm{C}}-U_{\beta}\cos\varphi_{\mathrm{C2}}>0\\ \varphi_{\mathrm{k}}-\frac{\pi}{2} & \text{when } U_{\mathrm{cg}}\cos\varphi_{\mathrm{C}}-U_{\beta}\cos\varphi_{\mathrm{C2}}<0\end{cases}. \tag{24}$$

According to (16), θ_{B} can be obtained

$$\theta_{\mathrm{B}}=\arctan\left(\frac{I_{\mathrm{a}}\sin\theta_{\mathrm{A}}}{I_{\mathrm{c}}-I_{\mathrm{a}}\cos\theta_{\mathrm{A}}}\right). \tag{25}$$

Substituting I_{a}, θ_{A}, and θ_{B} into (17), I_{b} can be obtained. So far, the reference values of the input currents can be calculated. This reference value is a function of the phase shift angle θ_{AC}, and the reference value of the input currents can be adjusted according to the change of the phase shift angle θ_{AC}.

2) DC Voltage Control: In the previous analysis, based on the input and output power balance equation, the current reference value of the input side is calculated. However, due to various factors such as measurement accuracy and control accuracy, it is difficult to achieve complete power balance. After time accumulation, it may cause dc voltage deviation. In order to increase the dc voltage correction capability, dc voltage control is introduced. The key to the control of dc voltage is to control the input and output power of the converter. Since the relationship of power balance is determined in (9), in order to control the dc voltage, a power difference should be generated between the input power and the output power. It is assumed that the output power is m times of the input power, where $m>0$.

$$m\left(U_{\alpha}I_{\mathrm{a}}\cos\varphi_{\mathrm{A}}+U_{\beta}I_{\mathrm{b}}\cos\varphi_{\mathrm{B}}\right)=U_{\mathrm{cg}}I_{\mathrm{c}}\cos\varphi_{\mathrm{C}} \tag{26}$$

$$\cos\varphi_{\mathrm{C}}{}'=\frac{\cos\varphi_{\mathrm{C}}}{m}. \tag{27}$$

Therefore, the variable m can be introduced into the expression by replacing $\cos\varphi_{\mathrm{C}}$ with $\cos\varphi'_{\mathrm{C}}$ in (9). The reference current $\dot{I}_{\mathrm{a}}$ and $\dot{I}_{\mathrm{b}}$ obtained according to the algorithm is containing the power adjustment parameter m, so that the input power can be controlled. In traction condition, when the dc voltage is higher than the reference value, set $m>1$ to reduce the input power; when the dc voltage is lower than the reference value, set $m<1$ to increase the input power.

3) Control Strategy: When the system is in ANSPS mode, the overall three-leg cooperative control strategy is shown in Fig. 8. After the dc voltage difference passes through the PI controller, the result is subtracted by 1 to obtain the power adjustment parameter m. It is input into the decoupling control with voltage, current, and angle information to obtain the reference value of input current, and the calculation flowchart of decoupling control is shown in Fig. 9. The currents of the leg a and leg b adopt deadbeat control to track their respective current reference values. The virtual midpoint potential is at the circumcenter of the triangle formed by the traction feeder voltages, as shown in Fig. 6(b), the virtual midpoint potential reference value is expressed as $u^*_{\mathrm{og}}=1/3(u\alpha+u\beta)$. The PWM pulses, G_{a}, G_{b}, and G_{c}, generated by this control method, act on the bridge legs a, b, and c, respectively.

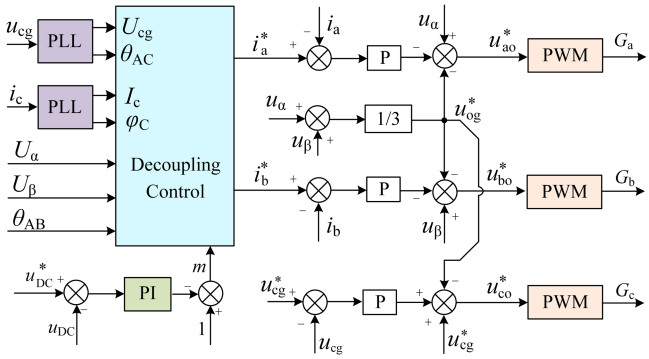

Fig. 8. Control strategy of ANSPS mode.

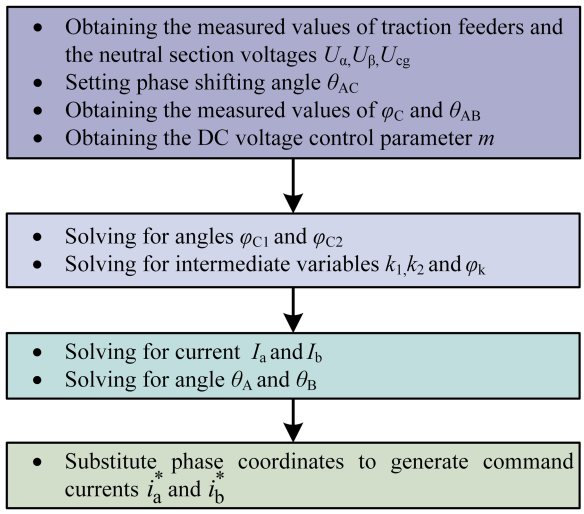

Fig. 9. Calculation flowchart of decoupling control.

B. RPC Mode

1) Operation Principle: During this stage, the locomotive is located in the traction feeder, and the objective of converter control is to compensate for the currents on the grid side, thereby balancing the three-phase currents of the power grid. To prevent ambiguity, the compensation currents for the α and β phases are referred to as $\dot{I}_{\alpha\mathrm{c}}$ and $\dot{I}_{\beta\mathrm{c}}$, respectively. The equivalent model of the system is shown in Fig. 5(b).

In the following, the selection of the virtual midpoint potential reference value is introduced first, and then the compensation currents $\dot{I}_{\alpha\mathrm{c}}$ and $\dot{I}_{\beta\mathrm{c}}$ are calculated. The phasor diagram of the system without compensation is shown in Fig. 10 with the voltage of traction feeder α as the phase angle reference zero. The traction feeder voltages approximately form an equilateral triangle. The reference value for the virtual midpoint potential should be chosen at the circumcenter of the triangle, as shown in Fig. 6(b). Since the c-phase leg is time-division multiplexed, when the system is in the RPC mode, the c-phase leg constitutes a ground path, so it must bear the potential U_{og}, and the output voltage of phase c leg is $\dot{U}_{\mathrm{co2}}$.

Since the locomotives in the electrified railway are mainly ac–dc–ac electric locomotives, this kind of electric locomotive is selected as an example to illustrate the principle of RPC. The

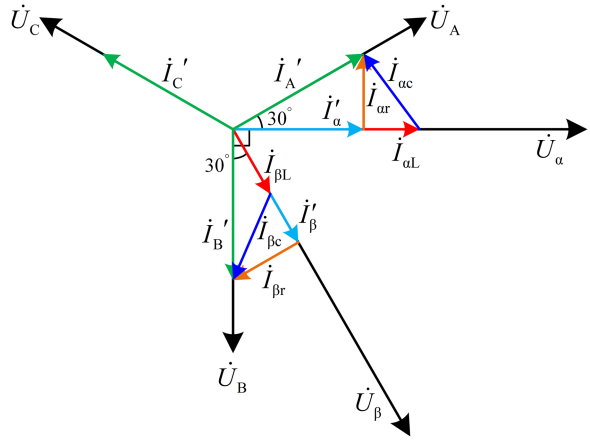

Fig. 10. Phasor diagram of system after compensation.

power factor is nearly 1. Thus, the load currents $\dot{I}_{\alpha L}$ is in phase with the traction feeder voltage $\dot{U}_\alpha$, and $\dot{I}_{\beta L}$ is in phase with the traction feeder voltage $\dot{U}_\beta$. The system compensation currents are divided into two parts: the active current transfer and the reactive current compensation. First, the system shifts half of the active current difference of the two sections from the heavily loaded section to the lightly loaded section. Taking the load situation in Fig. 10 as an example, the system shifts ΔI from phase α to phase β.

$$\Delta I = 0.5\left|I_{\alpha L} - I_{\beta L}\right|. \tag{28}$$

The output currents of the traction transformer after the active current transfer are $\dot{I}_\alpha$ánd $\dot{I}_\beta$.

Subsequently, to achieve a balanced three-phase load on the grid, additional reactive currents need to be introduced to phase α and phase β. The reactive currents compensated to the phase α and phase β are $\dot{I}_{\alpha r}$ and $\dot{I}_{\beta r}$. Therefore, the total compensation currents are the sum of the above-mentioned two parts of compensation, expressed as $\dot{I}_{\alpha c}$ and $\dot{I}_{\beta c}$. After the compensation, the three-phase currents on the grid side are $\dot{I}_A$, $\dot{I}_B$ánd $\dot{I}_C$, as illustrated in Fig. 10.

2) Control Strategy: In the previous RPC mode theory analysis, ac–dc–dc electric locomotive with power factor of approximately 1 is taken as an example. However, in practice, there are still a few ac–dc electric locomotives in the railway with lower power factors. Consequently, during the active current transfer, the transferred active current cannot simply be added or subtracted using the traction feeder current. In the RPC control, the total active current of the system should be extracted first. Subsequently, the active current is distributed to the three phases of the power grid by the converter, ensuring that the power factor on the grid side remains at 1. The multiplication of the traction feeder voltage and current is passed through a low-pass filter to obtain the dc component I_p, which represents the active current.

This active current is superimposed on the current maintaining the dc voltage to obtain $\dot{I}_A$ín phase A of the grid and $\dot{I}_B$ín phase B of the grid, according to Fig. 10. On this basis, the compensating currents of the converter are obtained by subtracting them from the load currents of the traction feeders. The

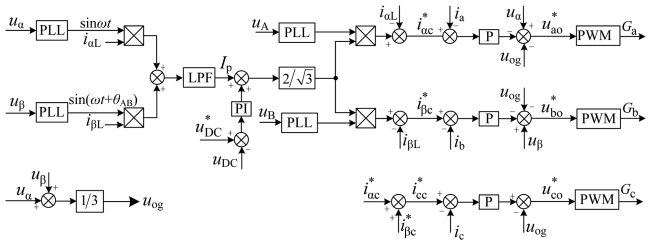

Fig. 11. Control strategy of RPC mode.

virtual midpoint potential is still located in the circumcenter of the two traction feeder voltages as indicated in Fig. 6(b). The virtual midpoint potential reference value is expressed as $u_{og}^* = 1/3(u\alpha + u\beta)$. The control strategy of the RPC mode is shown in Fig. 11. The PWM pulses, G_a, G_b, and G_c, generated by this control method, act on the bridge legs a, b, and c, respectively.

C. Transition Timing of the Two Modes

Using the transition of the train from traction feeder α to β as an illustration, where the traction current of the train is represented as $\dot{I}_{\text{load}}$, and the currents of traction feeders are denoted as $\dot{I}_{\alpha L}$ and $\dot{I}_{\beta L}$, while the output current of the ANSPS converter is $\dot{I}_c$.

T_{P1}–T_{P8} represent the moments when the locomotive is positioned at points P_1–P_8. Upon the train reaching point P_1, the system switches from the RPC mode to the ANSPS mode. While the train is positioned between P_1 and P_2, the converter is in no-load rectification, and the inverter side is also no-load inverter, waiting for the train's arrive at P_2. When located in the P_2–P_3 sections, the locomotive pantograph simultaneously overlaps the neutral section and the traction feeder, transferring the locomotive load current from the traction feeder to the converter. To mitigate the overvoltage at P_3, it is essential to transfer the load current from the traction feeder to the converter gradually before the train's arrival at P_3. The reference value for the output current $\dot{I}_c$ of the converter is given by

$$\dot{I}_c^* = \begin{cases} 0 & t < T_{P2} \\ \frac{(t-T_{P2})}{T_{\text{trans}}}\dot{I}_{\text{load}} & T_{P2} < t < T_{P2} + T_{\text{trans}} \\ \dot{I}_{\text{load}} & T_{P2} + T_{\text{trans}} < t < T_{P3} \end{cases} \tag{29}$$

where T_{trans} represents the current transfer time. At this stage, the output current amplitude of the converter rises gradually.

When the train is in the P_3–P_6 section, the converter needs to provide an output voltage that is adjustable in both amplitude and phase. The reference value of the neutral section catenary voltage is u_c^*, which is adjusted according to the position of the train.

$$u_c{}^* = \begin{cases} \sqrt{2}U_\alpha \sin(\omega t)\, T_{P3} \le t < T_{P4} \\ \sqrt{2}U_\alpha \sin\left(\omega t + \frac{(t-T_{P4})}{T_{\text{shift}}}\theta_{AB}\right) T_{P4} \le t < T_{P4} + T_{\text{shift}} \\ \sqrt{2}U_\alpha \sin(\omega t + \theta_{AB})\, T_{P4} + T_{\text{shift}} \le t < T_{P6} \end{cases} \tag{30}$$

where T_{shift} is the phase shift time of the voltage from phase α to phase β. In the P_6–P_7 section, similar to the P_2–P_3 section, it is

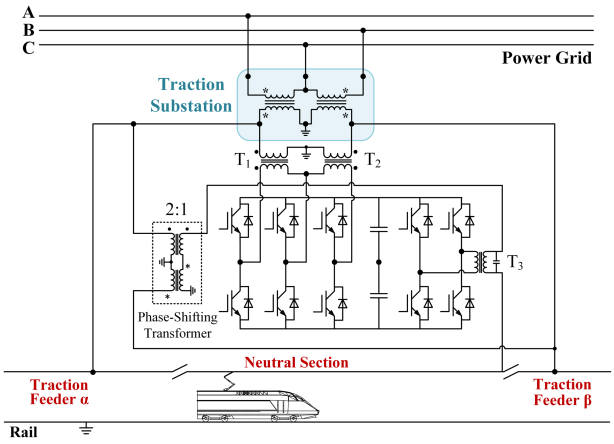

Fig. 12. Configuration of automatic neutral section power system (Scheme 2).

essential to gradually transfer the load current from the converter to the traction feeder. The reference value for converter output current is denoted as follows:

$$\dot{I}_{\mathrm{c}}^{*}=\begin{cases}\dot{I}_{\mathrm{load}} & T_{\mathrm{P3}}\le t<T_{\mathrm{P6}}\\ \left(1-\frac{(t-T_{\mathrm{P6}})}{T_{\mathrm{trans}}}\right)\dot{I}_{\mathrm{load}} & T_{\mathrm{P6}}\le t<T_{\mathrm{P6}}+T_{\mathrm{trans}}\\ 0 & T_{\mathrm{P6}}+T_{\mathrm{trans}}\le t\end{cases}. \quad (31)$$

When the train is located between P_7 and P_8, the converter is in no-load rectification, and the inverter side is also no-load inverter, waiting for the train to leave P_8. As the train reaches the P_8 point, the system switches from the ANSPS mode to the RPC mode.

IV. Scheme Comparison

The cost of the power electronic converter mainly depends on the capacity of the power electronic device. In this part, a cost-effective ANSPS [24] and a typical RPC [18] are selected for the power electronics capacity comparison with the converter topology proposed in this article. In the comparison of multiple topologies, the product of the withstand voltage and current capability of the bridge leg is selected for comparison. The phase angle difference between the two traction feeder voltages is $\pi/3$. The voltage amplitude of the traction feeders is U_{T}, and the amplitude of the locomotive traction current is I_{T}.

For the topology proposed in this article, the circuit topology is shown in Fig. 2, and the phasor diagram is shown in Fig. 6(b), which is abbreviated as **Scheme 1**. The virtual neutral point potential is selected as the circumcenter of the triangle formed by the traction feeder voltages. The output voltage amplitude of each leg is $\sqrt{3}/3\,U_{\mathrm{T}}$. The leg currents are determined by the locomotive traction current. The minimum current capacity for each bridge leg is I_{T}. Therefore, the minimum converter capacity, denoted as S_1, in **Scheme 1** is given by

$$S_1\ge 3\times\frac{\sqrt{3}}{3}U_{\mathrm{T}}\times I_{\mathrm{T}}\approx 1.73U_{\mathrm{T}}I_{\mathrm{T}}. \quad (32)$$

The cost-effective ANSPS with different topology is shown in Fig. 12, which is abbreviated as **Scheme 2**. The phase-shifting transformer is used to reduce the output voltage of the inverter side. The ratio of the primary and secondary sides of the phase-shifting transformer is 2:1. The secondary side is connected in series, and the phase-shifting transformer voltage $\dot{U}_{\mathrm{ps}}$ is given by

$$\dot{U}_{\mathrm{ps}}=\frac{1}{2}\left(\dot{U}_{\alpha}+\dot{U}_{\beta}\right). \quad (33)$$

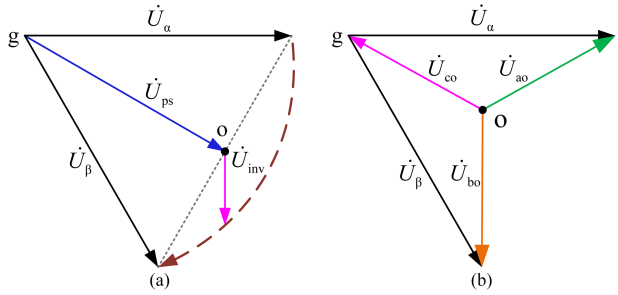

Fig. 13. Phasor diagram of Scheme 2 (a) in the inverter side and (b) in the rectifier side.

For the topology proposed in Fig. 12, the phase diagram of the inverter side is shown in Fig. 13(a). The transformer on the inverter side is T_3, and its high-voltage side output voltage is $\dot{U}_{\mathrm{inv}}$. This voltage is superimposed with $\dot{U}_{\mathrm{ps}}$ to supply power to the neutral section. The maximum output voltage amplitude of each phase is $0.25U_{\mathrm{T}}$. The minimum current capacity for each leg is I_{T}. Therefore, the minimum capacity of the inverter side S_{2_inv} is

$$S_{2\_\mathrm{inv}}\ge\frac{1}{4}U_{\mathrm{T}}\times I_{\mathrm{T}}\times 2=0.5U_{\mathrm{T}}I_{\mathrm{T}}. \quad (34)$$

Since the power of the transformer flowing into the transformer is equal to the power flowing out of the transformer, the ratio of transformer does not affect the result of power electronic device capacity comparison. When the inductance voltage drop is ignored, the phase diagram of the rectifier side is shown in Fig. 13(b). If **Schemes 1** and **2** have the same power quality management ability, the minimum capacity of the rectifier side S_{2_ref} needs to be at least the same as S_1.

$$S_{2\_\mathrm{rec}}\ge 3\times\frac{\sqrt{3}}{3}U_{\mathrm{T}}\times I_{\mathrm{T}}\approx 1.73U_{\mathrm{T}}I_{\mathrm{T}}. \quad (35)$$

If considering that the rectifier side also needs to transmit active power for the inverter side, the capacity should need to be larger on the rectifier side. Combining (34) and (35), the total converter capacity S_2 is

$$S_2=S_{2\_\mathrm{inv}}+S_{2\_\mathrm{rec}}\ge 2.23U_{\mathrm{T}}I_{\mathrm{T}}. \quad (36)$$

The typical RPC is shown in Fig. 14, which is abbreviated as **Scheme 3**. When the inductance voltage drop is ignored, the phase diagram of the RPC is shown in Fig. 15. If **Schemes 3** and **1** have the same power quality management ability, the capacity of RPC S_3 needs to be the same as S_1.

$$S_3\ge 3\times\frac{\sqrt{3}}{3}U_{\mathrm{T}}\times I_{\mathrm{T}}\approx 1.73U_{\mathrm{T}}I_{\mathrm{T}}. \quad (37)$$

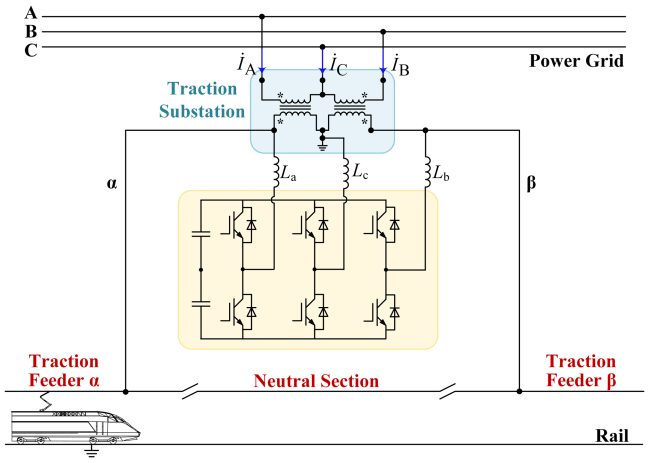

Fig. 14. Configuration of RPC (Scheme 3).

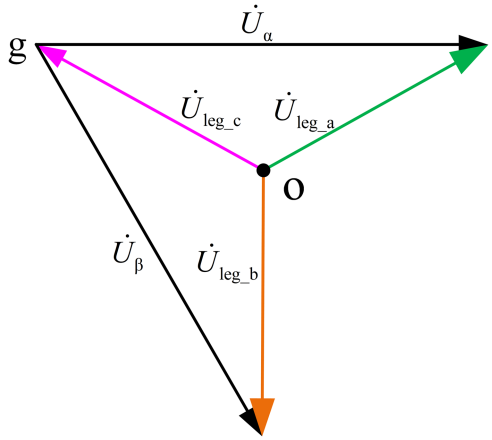

Fig. 15. Phasor diagram of Scheme 3.

TABLE I
CAPACITY COMPARISON

Scheme	Circuit topology diagram	Function	Minimum capacity
1	Fig. 2 (Proposed in article)	Neutral section power supply and RPC	$1.73U_TI_T$
2	Fig. 12	Neutral section power supply and RPC	$2.23U_TI_T$
3	Fig. 14	RPC	$1.73U_TI_T$

The comparison of these three schemes is shown in Table I.

V. SIMULATION RESULTS

In this section, the control of the whole process of the automatic neutral section power system is tested based on MATLAB/Simulink. The main parameters of the circuit are shown in Table II. The locomotive load (9600 kW) is equivalent to a CPC current source.

TABLE II
MAIN PARAMETERS

Parameters	Values	Parameters	Values
U_α(kV)	27.5	L_a(mH)	10
U_β(kV)	27.5	L_b(mH)	10
θ_{AB}(deg)	60	L_c(mH)	10
U_{dc} (kV)	45	C(mF)	5
Rated power(kW)	9600	Rated load current (A)	350

TABLE III
TIME SEQUENCE PARAMETERS OF ANSPS

Positions	Time(s)	Positions	Time(s)
P_1–P_2	0.0–0.3	P_5–P_6	2.0–2.4
P_2–P_3	0.3–0.6	P_6–P_7	2.4–2.7
P_3–P_4	0.6–1.0	P_7–P_8	2.7–3.0
P_4–P_5	1.0–2.0		

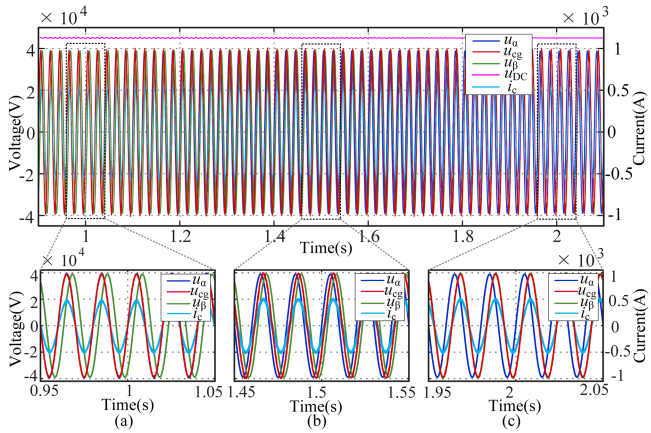

Fig. 16. Simulation waveform of output voltages and current. (a) Simulation waveform before the phase shift. (b) Simulation waveform when neutral section voltage at 30° phase shift. (c) Simulation waveform after the phase shift.

A. ANSPS Mode

In this mode, the train is located between P_1 and P_8. When the locomotive is located in P_2–P_3 or P_6–P_7 in Fig. 5, the time of the simultaneous overlap process is T_{trans}, which is set to 0.3 s in the simulation. When the locomotive is located in P_4–P_5, the output voltage is phase shifted, and the phase shift time is the T_{shift}, which is set to 1 s. The time sequence parameters are shown in Table III.

1) Under the Conventional Traction Condition of Locomotive: Under the conventional traction condition, the locomotive runs at a constant power under the condition that the power factor is approximately 1. Based on the circuit parameters in Tables II and III, the simulation is carried out with the train moving from traction feeder α to β.

When the train is located between P_3 and P_6, the output voltage of the system supplies power to the train in the neutral section, the simulation result is shown in Fig. 16. The output

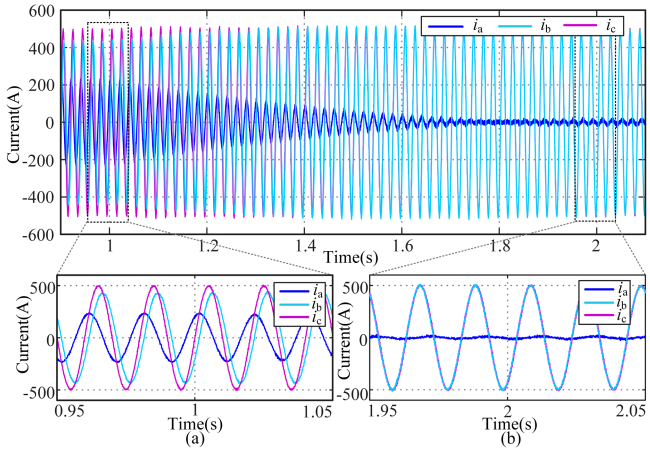

Fig. 17. Current simulation waveform. (a) Output currents of three legs before phase shift. (b) Output currents of three legs after phase shift.

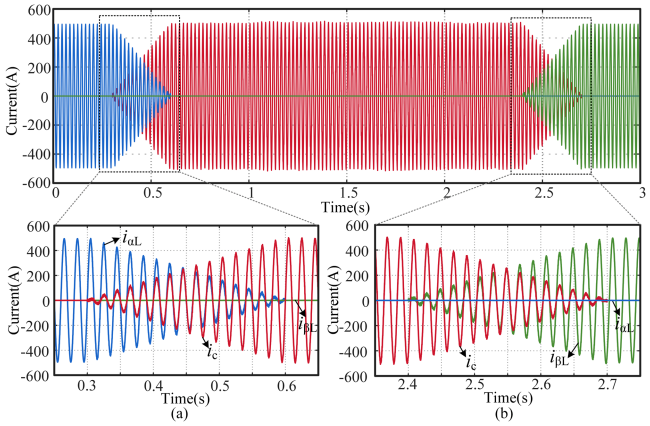

Fig. 18. Current simulation waveform. (a) Traction current is transferred from the traction feeder α to the output current of converter. (b) Traction current is transferred from the output current of converter to the traction feeder β.

voltage starts to shift from the voltage of traction feeder α to the voltage of traction feeder β at 1 s, and the phase shift process ends at 2 s. Fig. 16(a) shows the simulation waveform before the phase shift of the neutral section voltage u_{cg}, and the neutral section voltage u_{cg} coincides with the voltage of traction feeder α. Fig. 16(b) shows the simulation waveform when the neutral section voltage u_{cg} at 30° phase shift, u_{cg} is located in the middle of the two traction feeder voltages. Fig. 16(c) shows the simulation waveform after the phase shift, and the neutral section voltage u_{cg} coincides with the voltage of traction feeder β. It can be seen from the diagram that the neutral section voltage transits smoothly between the two traction feeder voltages. During this process, the dc voltage is kept constant.

The output currents of three legs are shown in Fig. 17. Fig. 17(a) shows the output currents of three legs before phase shift. Fig. 17(b) shows the output currents of three legs after phase shift. With the change of the neutral section voltage u_{cg}, the output current of b leg gradually increases and the output current of a leg gradually decreases. During the whole phase shift process, the output currents of phase a leg and phase b leg are always not greater than the output current of phase c leg.

When the locomotive is located in the P_2–P_3 or P_6–P_7 sections, the system transfers the traction current, the simulation result of the current transfer process is shown in Fig. 18. When the locomotive is located in the P_2–P_3. The traction current is transferred from the traction feeder α to the output current of phase c leg i_c, the output current of phase c leg increases slowly from zero, as shown in Fig. 18(a). When the locomotive is located in the P_6–P_7, the traction current is transferred from the output current of phase c leg to the traction feeder β, the output current of phase c leg decreases gradually to zero, as shown in Fig. 18(b). It can be seen from Fig. 18 that the traction current is smoothly transferred, and the traction current transfer process is consistent with the rules of (29) and (31). In this process, the leg current waveforms are shown in Fig. 19.

2) Under Various Traction Conditions of Locomotive: Next, the system will be simulated in three different traction conditions.

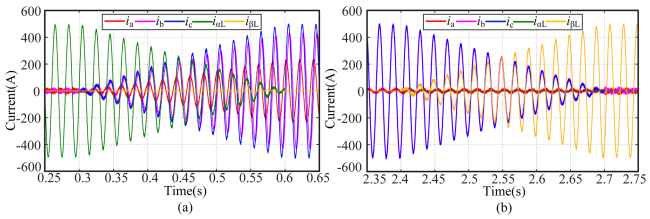

Fig. 19. Current simulation waveform. (a) Phase leg currents when located between P_2 and P_3. (b) Phase leg currents when located between P_6 and P_7.

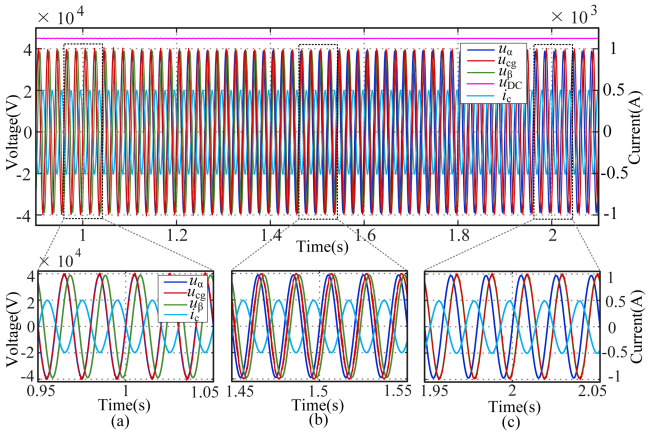

Fig. 20. Simulation waveform of output voltages and current under regenerative braking condition. (a) Simulation waveform before the phase shift. (b) Simulation waveform when neutral section voltage at 30° phase shift. (c) Simulation waveform after the phase shift.

Case 1: When the train is in the state of regenerative braking, the power flows from the locomotive to the traction feeder. The simulation waveform of the train under regenerative braking condition is shown in Fig. 20. The phase of locomotive traction voltage u_{cg} is opposite to that of traction current i_c. The output voltage can still be smoothly transferred between the two traction feeder voltages. The system proposed in this article considers the regenerative braking condition and the dc voltage is kept constant.

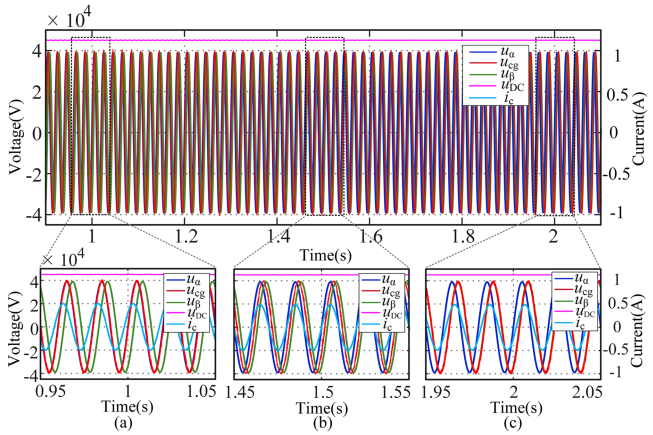

Fig. 21. Simulation waveform of output voltages and current taking AC/DC drive electric locomotive as load. (a) Simulation waveform before the phase shift. (b) Simulation waveform when neutral section voltage at 30° phase shift. (c) Simulation waveform after the phase shift.

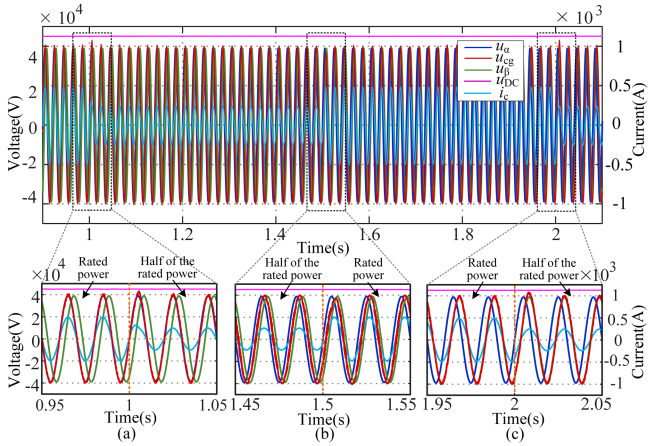

Fig. 22. Simulation waveform of output voltages and current in the case of sudden change of traction power. (a) Simulation waveform before the phase shift. (b) Simulation waveform at 30° phase shift. (c) Simulation waveform after the phase shift.

Case 2: There are still a certain number of ac–dc drive electric locomotives in some railway lines and the power factor is generally only about 0.8 [6]. When the ac–dc drive electric locomotive is used as the load, the simulation waveform is shown in Fig. 21. The phase of locomotive traction voltage u_{cg} is ahead of traction current i_c.

Case 3: In order to verify the dynamic performance of the proposed system in this article, the locomotive is changed from full rated power to half of the rated power in a very short period of time in the simulation and the simulation result is shown in Fig. 22. When the simulation time is 1 and 2 s, the traction power changes from rated power to half of the rated power, the voltage of the catenary in the neutral section will increase slightly and fall back rapidly in half a cycle, as shown in Fig. 22(a) and (c). When the simulation time is 1.5 s, the traction power changes from half of the rated power to rated power, the voltage of the catenary in the neutral section will drop slightly, but it will recover quickly, as shown in Fig. 22(b). In the case of sudden change of traction power, the neutral section voltage is still smoothly transferred between the two traction feeder voltages.

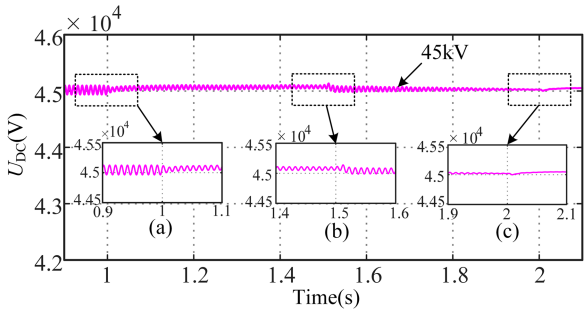

Fig. 23. DC voltage simulation waveform.

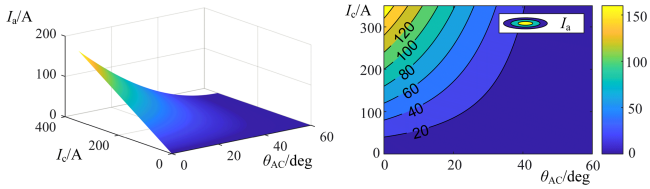

Fig. 24. Simulation result of variation of I_a with phase shift angle and load current when the power factor is 0.98.

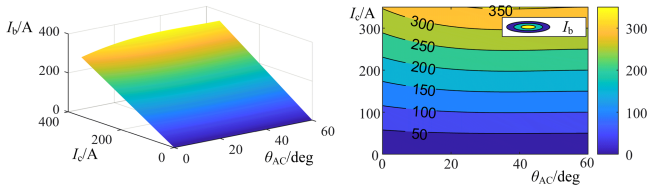

Fig. 25. Simulation result of variation of I_b with phase shift angle and load current when the power factor is 0.98.

In the case of sudden change of traction power, the simulation waveform of dc voltage is shown in Fig. 23. In this process, the dc voltage is basically constant. The maximum ripple amplitude of the dc voltage is about 100 V. When the traction power changes from rated power to half of the rated power, the dc voltage ripple increases, as shown in Fig. 23(a) and (c). When the traction power changes from half of the rated power to rated power, the dc voltage ripple decreases, as shown in Fig. 23(b).

3) Variation of I_a *and* I_b *With Load Current* I_c *and Phase Shift Angle* θ_{AC}*:* During the phase shift process (P_3–P_6), the input current amplitude I_a and I_b will also change. When the locomotive power factor is 0.98, the variation of I_a with the load current and the phase shift angle is shown in Fig. 24, and the variation of I_b with the load current and phase shift angle is shown in Fig. 25. When the locomotive power factor is 0.8, the variation of I_a with the load current and the phase shift angle is shown in Fig. 26, and the variation of I_b with the load current and the phase shift angle is shown in Fig. 27.

It can be seen from these figures that the input current amplitude will increase with the load current when the phase

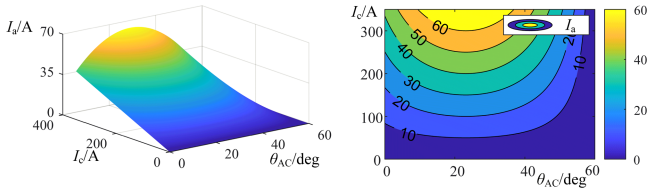

Fig. 26. Simulation result of variation of I_a with phase shift angle and load current when the power factor is 0.8.

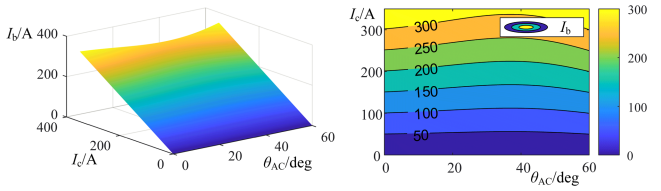

Fig. 27. Simulation result of variation of I_b with phase shift angle and load current when the power factor is 0.8.

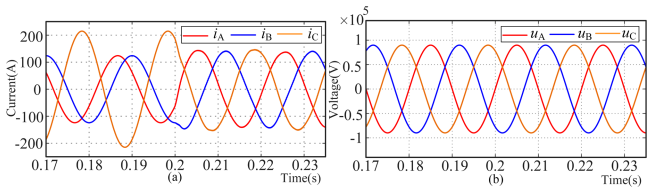

Fig. 28. Simulation waveform in RPC mode. (a) Waveform of the three-phase currents in grid. (b) Waveform of the three-phase voltages in grid.

shift angle is the same; the input current amplitude will vary with the phase shift angle when the load current is the same. By comparing Fig. 24 with Figs. 26 and 25 with Fig. 27, the variation pattern of the input currents with the phase shift angle varies under different load power factors. Further analysis of the change process from these diagrams shows that the input current amplitude does not exceed the load current throughout the phase shift process. Therefore, when calculating the converter capacity, the current capacity of each leg is designed according to the maximum load current.

B. RPC Mode

When there is an electric locomotive in traction feeder α and there is also an electric locomotive in traction feeder β, the system is in RPC mode, the simulation waveform is shown in Fig. 28. Before 0.2 s, the three-phase currents in power grid are unbalanced, there is a phase difference between currents and voltages, and the power factor is low. At 0.2 s, the converter starts to operate and the amplitude of the three-phase currents are equal, and the power factor is 1.

VI. Experimental Results

In order to further verify the effectiveness and the superiority of the devices and control strategies proposed in this article, a corresponding scaled-down experimental prototype is built as shown in Fig. 29. Its main parameters are shown in Table IV.

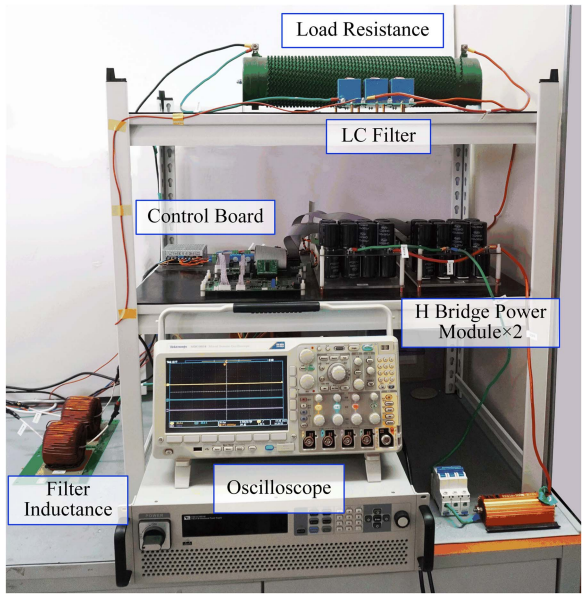

Fig. 29. Photograph of scaled-down experimental prototype.

TABLE IV
Main Parameters of Experimental Prototypes

Parameters	Values	Parameters	Values
Voltage of traction feeder α	220 V	Phase of traction feeder α	0°
Voltage of traction feeder β	220 V	Phase of traction feeder β	−60°
Voltage of neutral section	220 V	DC voltage	400 V
Branch inductor	5 mH	Capacitor in dc side	4.84 mF
Load resistance	25 Ω	Switching frequency	10 kHz

The prototype is powered by a three-phase power grid, in which two line voltages are used to simulate the traction feeder voltages. The RMS values of the voltages in the traction feeders are 220 V, and the voltage phase difference between the two traction feeders is 60°. The main power circuit is a three-phase converter built on two full-bridge power modules, one of which uses only one leg. The switching frequency of the H-bridge is 10 kHz, the control frequency is set to 10 kHz, and the phase-locked loop is used to obtain the phases of the voltages and currents.

When the neutral section voltage is switched from the traction feeder α to the traction feeder β, the experimental results are shown in Fig. 30. The phase shift time is set to 1 s, the phase shift begins at 0.2 s, and the phase shift process ends at 1.2 s. Fig. 30(a) shows the experimental waveforms before the phase shift. The neutral section voltage before the phase shift is consistent with the voltage of traction feeder α. Fig. 30(b) shows the experimental waveform at 30° phase shift, with the neutral section voltage between the traction feeder α and traction

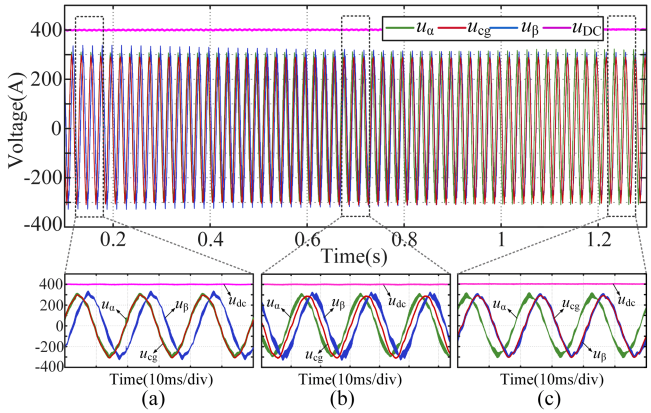

Fig. 30. Voltage waveforms in the experiment. (a) Neutral section voltage before the phase shift. (b) Neutral section voltage at a 30° phase shift. (c) Neutral section voltage after the phase shift.

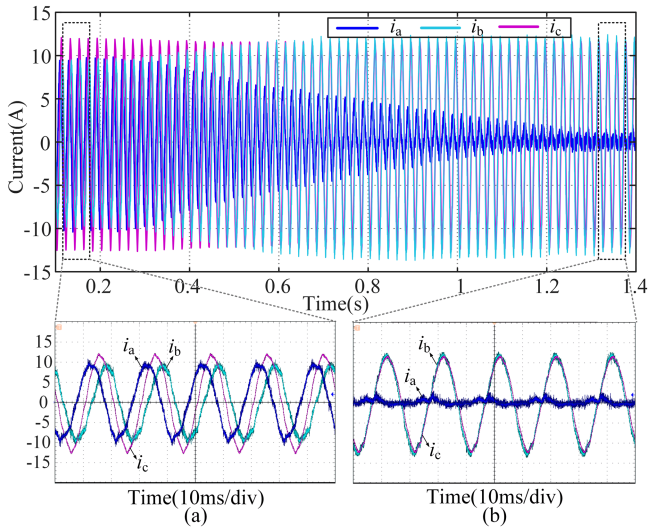

Fig. 31. Current waveforms in the experiment. (a) Input current waveform before the phase shift. (b) Input current waveform after the phase shift.

feeder β voltages. Fig. 30(c) shows the experimental waveforms after the phase shift. The neutral section voltage after the phase shift is consistent with the voltage of traction feeder β. The experimental results show that the neutral section voltage can be smoothly transitioned, with the dc voltage remaining at 400 V during this period.

When the neutral section voltage is switched from the traction feeder α to the traction feeder β, the waveforms of output currents of the three legs in the experiment are shown in Fig. 31. The phase shift time is set to 1 s, the phase shift starts at 0.2 s and the phase shift process ends at 1.2 s. As the phase shift angle increases, the output current of leg a gradually decreases and output current of leg b gradually increases, which is the same as the simulation results in Section V. The amplitude of input currents I_a and I_b does not exceed the load current throughout the phase shift process.

In order to show the voltage and current change process more clearly, the phase shift time is set to 0.1 s. The voltage waveform in the experiment is shown in Fig. 32, and the current waveform in the experiment is shown in Fig. 33.

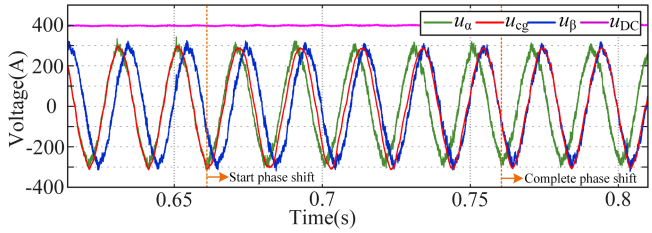

Fig. 32. Voltage waveforms in the experiment when the phase shift time is set to 0.1 s.

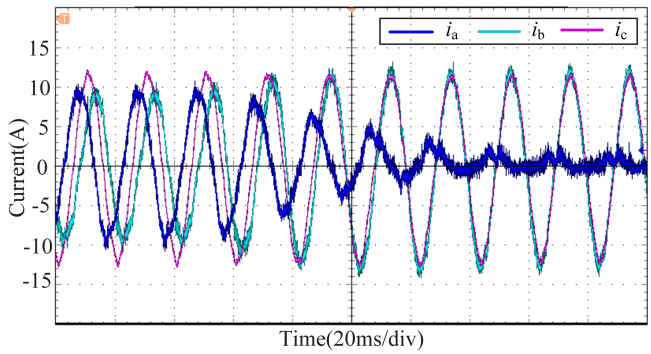

Fig. 33. Current waveforms in the experiment when the phase shift time is set to 0.1 s.

VII. Conclusion

A new converter topology for an ANSPS based on a three-leg converter is proposed in this article. This topology has fewer bridge-leg counts and requires a smaller converter capacity when used as an ANSPS. After adding an inductor and an ac switch, this converter can serve as an RPC, utilizing the idle time of the ANSPS on time-division basis to improve the power quality of the traction power supply. The utilization rate of the converter can be greatly improved by over 95%. Aiming at the coupling relationship of the topology in ANSPS mode, this article proposes a three-leg cooperative control method, which can accurately and quickly perform decoupling control. It has good transient control ability and is easy to maintain dc voltage constant. The topology scheme proposed in this article improves the economy and practicality of the ANSPS system.

References

[1] M. Brenna, F. Foiadelli, and H. J. Kaleybar, "The evolution of railway power supply systems toward smart microgrids: The concept of the energy hub and integration of distributed energy resources," *IEEE Electrific. Mag.*, vol. 8, no. 1, pp. 12–23, Mar. 2020.

[2] S. M. M. Gazafrudi, A. Tabakhpour Langerudy, E. F. Fuchs, and K. Al-Haddad, "Power quality issues in railway electrification: A comprehensive perspective," *IEEE Trans. Ind. Electron.*, vol. 62, no. 5, pp. 3081–3090, May 2015.

[3] Q. Xu et al., "Analysis and comparison of modular railway power conditioner for high-speed railway traction system," *IEEE Trans. Power Electron.*, vol. 32, no. 8, pp. 6031–6048, Aug. 2017.

[4] Z. Li, X. Li, Y. Wei, C. Lu, Y. Lin, and Z. Li, "Ground fault analysis and grounding method of static power converters in flexible AC traction power supply systems," *IEEE Trans. Power Electron.*, vol. 37, no. 5, pp. 5535–5546, May 2022.

[5] Q. Wang, J. Lu, Q. Wang, and J. Duan, "Transient overvoltage study of auto-passing neutral section in high-speed railway," in *Proc. IEEE Transp. Electrific. Conf. Expo, Asia-Pacific*, 2017, pp. 1–5.

[6] Z. Zhang et al., "Smart electric neutral section executer embedded with automatic pantograph location technique based on voltage and current signals," *IEEE Trans. Transp. Electrific.*, vol. 6, no. 3, pp. 1355–1367, Sep. 2020.
[7] Z. Zhang, K. Li, Z. Zhang, T. Q. Zheng, R. Hao, and X. You, "A thyristor-based auto-passing neutral section scheme with auxiliary transformers for AC electrified railway," *IEEE Trans. Transp. Electrific.*, vol. 9, no. 2, pp. 2296–2307, Jun. 2023.
[8] L. Liu, N. Dai, K. W. Lao, and W. Hua, "A co-phase traction power supply system based on asymmetric three-leg hybrid power quality conditioner," *IEEE Trans. Veh. Technol.*, vol. 69, no. 12, pp. 14645–14656, Dec. 2020.
[9] B. Chen, C. Zhang, C. Tian, J. Wang, and J. Yuan, "A hybrid electrical magnetic power quality compensation system with minimum active compensation capacity for V/V co-phase railway power supply system," *IEEE Trans. Power Electron.*, vol. 31, no. 6, pp. 4159–4170, Jun. 2016.
[10] X. He et al., "Advanced co-phase traction power supply system based on three-phase to single-phase converter," *IEEE Trans. Power Electron.*, vol. 29, no. 10, pp. 5323–5333, Oct. 2014.
[11] M. Straka, M. Pittermann, and V. Blahnik, "Topologies for cooperation of 25kV traction substations with rail active balancer and phase shifting device," in *Proc. IEEE 31st Int. Symp. Ind. Electron.*, 2022, pp. 354–359.
[12] S. Wu, M. Wu, L. Li, S. Wang, K. Song, and Y. Wang, "Analysis and comparison of MMC-based co-phase traction power supply topology for AT power supply system," *IEEE Trans. Power Del.*, vol. 27, no. 55, pp. 4053–4063, Oct. 2022.
[13] S. Cheng et al., "Structure improvement and control algorithm optimization based ground automatic neutral-section passing method for train," *IEEE Trans. Emerg. Sel. Topics Power Electron.*, vol. 11, no. 3, pp. 2879–2894, Jun. 2023.
[14] X. Tian, Q. Jiang, and Y. Wei, "Research on novel uninterruptible phase-separation passing scheme in electrified railways," *Power Syst. Protection Control*, vol. 40, no. 21, pp. 14–18, Nov. 2012.
[15] X. Tian, Q. Jiang, and Y. Wei, "Two-phase modular multilevel converter topology study of railway uninterruptible phase-separation passing device," *Power Syst. Technol.*, vol. 39, no. 10, pp. 2901–2906, Oct. 2015.
[16] X. Tian, Q. Jiang, and Y. Wei, "Research on novel railway uninterruptible flexible connector with series-connected transformers and back-to-back converter," in *Proc. IEEE ECCE Asia Downunder*, 2013, pp. 111–116.
[17] M. Lei, Y. Wang, and C. Zhao, "Optimized operation of the full-bridge five-branch modular multilevel converter for power quality enhancement of cophase railway power system," *IEEE Trans. Transp. Electrific.*, vol. 8, no. 1, pp. 590–604, Mar. 2022.
[18] H. M. Roudsari, A. Jalilian, and S. Jamali, "Flexible fractional compensating mode for railway static power conditioner in a V/v traction power supply system," *IEEE Trans. Ind. Electron.*, vol. 65, no. 10, pp. 7963–7974, Oct. 2018.
[19] F. Ma et al., "A railway traction power conditioner using modular multilevel converter and its control strategy for high-speed railway system," *IEEE Trans. Transp. Electrific.*, vol. 2, no. 1, pp. 96–109, Mar. 2016.
[20] M. Lei and Y. Wang, "A transformerless railway power quality compensator based on cascaded H-bridge featuring reduced branch capacity requirement," *IEEE Trans. Power Del.*, vol. 37, no. 6, pp. 5443–5453, Dec. 2022.
[21] Z. Ni et al., "Multi-function uninterrupted phase-separation passing system and its control method," *CSEE J. Power Energy Syst.*, vol. 9, no. 6, pp. 2332–2343, Nov. 2023.
[22] Y. Huang, H. Hu, Y. Wang, Y. Ge, and Y. Gu, "Flexible uninterrupted phase-separation passing system and its control strategy for electrified railway trains," *Trans. China Electrotechnical Soc.*, vol. 36, no. 23, pp. 4959–4969, Dec. 2021.
[23] Y. Wang et al., "A novel multifunctional power flow control system and its control strategy in section post for electrified railway," *Proc. CSEE*, Jun. 2023. [Online]. Available: http://kns.cnki.net/kcms/detail/11.2107.tm.20230616.1656.027.html
[24] W. Wang, Z. Li, C. Zhao, Y. Hu, and Y. Li, "Research on partial capacity phase-separation passing equipment control strategy," *Proc. CSEE*, vol. 39, no. 5, pp. 1461–1470, Mar. 2019.
[25] Z. Li et al., "Active disturbance rejection control for static power converters in flexible AC traction power supply systems," *IEEE Trans. Energy Convers.*, vol. 37, no. 4, pp. 2851–2862, Dec. 2022.
[26] M. Chen, Y. Chen, Y. Chen, X. Dai, and L. Liu, "Unified power quality management for traction substation groups connected to weak power grids," *IEEE Trans. Power Del.*, vol. 37, no. 5, pp. 4178–4189, Oct. 2022.
[27] Z. Ni, F. Xiao, J. Yuan, and Y. Ke, "Research on uninterrupted phase-separation passing device based on three-phase MMC," in *Proc. IEEE PES Asia-Pacific Power Energy Eng. Conf.*, 2019, pp. 1–6.

Zhibo Zhang (Graduate Student Member, IEEE) was born in Tieling, China, in 1996. He received the B.S. degree in electrical engineering in 2019 from Beijing Jiaotong University, Beijing, China, where he is currently working toward the Ph.D. degree in power electronics with the School of Electrical Engineering.

His current research interests include railway electrification system and PWM converter.

Trillion Q. Zheng (Senior Member, IEEE) received the B.S. degree in electrical engineering from Southwest Jiaotong University, Chengdu, China, in 1986, and the M.S. and Ph.D. degrees in electrical engineering from Beijing Jiaotong University, Beijing, China, in 1992 and 2002, respectively.

He is currently a University Distinguished Professor with Beijing Jiaotong University. He is also the Director of the Center for Electric Traction, Beijing Jiaotong University, founded by the Ministry of Education, China. His current research interests include the power supplies and ac drives of railway traction systems, high-performance and low-loss power electronics systems, PV-based converters and control, active power filters, and power quality correction.

Dr. Zheng was the recipient of the Youth Award of Railway Science and Technology of Zhan Tianyou in 2005 and the Zhongda Scholar for power electronics and motor drive area by the Delta Environmental and Educational Foundation in 2007.

Changyu Gao (Graduate Student Member, IEEE) was born in Jinan, China, in 1997. He received the B.S. degree in electrical engineering from Shandong University of Science and Technology, Qingdao, China, in 2019. He is currently working toward the Ph.D. degree in electrical engineering with Beijing Jiaotong University, Beijing, China.

His current research interests include multiport dc–dc converters and solid-state-transformers.

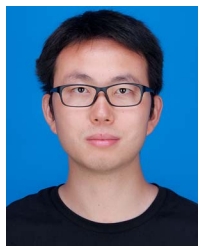

Kai Li (Member, IEEE) received the B.S. degree from Wuhan University, Wuhan, China, in 2011, and the Ph.D. degree from Tsinghua University, Beijing, China, in 2017, both in electrical engineering.

From 2013 to 2015, he was a Visiting Scholar with the Center for Power Electronics Systems, Virginia Tech, Blacksburg, VA, USA. From 2017 to 2019, he was a Postdoctoral Fellow with Tsinghua University. In 2019, he joined the School of Electrical Engineering, Beijing Jiaotong University, Beijing, China, where he is currently an Associated Professor with the School of Electrical Engineering.

His current research interests include solid-state transformer, railway electrification system, modular multilevel converters, and electrolytic hydrogen production converters.

Jiawei Guo was born in Cangzhou, China, in 1998. He received the B.S. and M.S. degrees in electrical engineering from Beijing Jiaotong University, Beijing, China, in 2020 and 2023, respectively.

His research interests include multilevel converters and railway electrification systems.